Published in final edited form as:
Biochemistry. 2011 December 20; 50(50): 10876–10886. doi:10.1021/bi2014745.

Secondary nucleating sequences affect kinetics and thermodynamics of tau aggregation

Christopher L. Moore[1], **Michael H. Huang**[1], **Shauna A. Robbennolt**[1], **Kellen R. Voss**[2], **Benjamin Combs**[2], **T. Chris Gamblin**[2], and **Warren J. Goux**[1,*]

[1]Department of Chemistry, The University of Texas at Dallas, 800 W. Campbell Rd., Richardson, TX 75080

[2]Department of Molecular Biosciences, University of Kansas, 1200 Sunnyside Ave., Lawrence, KS 66045

Abstract

Tau protein was scanned for highly amyloidogenic sequences in amphiphilic motifs $(X)_nZ$, $Z(X)_nZ$ (n≥2) or $(XZ)_n$ (n≥2), where X is a hydrophobic residue and Z is a charged or polar residue. N-acetyl peptides homologous to these sequences were used to study aggregation. Transmission electron microscopy (TEM) showed 7 peptides, in addition to well known primary nucleating sequences c^{275}VQIINK (AcPHF6*) and Ac^{306}VQIVYK (AcPHF6), formed fibers, tubes, ribbons or rolled sheets. Of the peptides shown by TEM to form amyloid, Ac^{10}VME, AcPHF6*, Ac^{375}KLTFR, and Ac^{393}VYK were found to enhance the fraction of β-structure of AcPHF6 formed at equilibrium, and Ac^{375}KLTFR was found to inhibit AcPHF6 and AcPHF6* aggregation kinetics in a dose-dependent manner, consistent with its participation in a hybrid steric zipper model. Single site mutants were generated which transformed predicted amyloidogenic sequences in tau into non-amyloidogenic ones. A M11K mutant had fewer filaments and showed a decrease in aggregation kinetics and an increased lag time compared to wild type tau, while a F378K mutant showed significantly more filaments. Our results infer that sequences throughout tau, in addition to PHF6 and PHF6*, can seed amyloid formation or affect aggregation kinetics or thermodynamics.

Tau is a microtubule-associated protein that regulates microtubule stability, neurite growth and other microtubule-dependent functions. The human protein exists as six isoforms, consisting of an acidic N-terminal containing up to two 29-amino acid inserts and a basic microtubule binding region (MTBR) containing either three or four tandem 31 (or 32) amino acid pseudo-repeats (R1–R4) near the C-terminal (1–4). Normal phosphorylation of tau by proline-directed kinases (GSK-3β, MAPK, CDK5) and by non-proline directed kinases (PKA, MARK, SADK, and Src family of tyrosine kinases) may affect tau's affinity for microtubules and regulate the dynamics of microtubules, establish neuronal polarity, axonal outgrowth and axonal transport in mature neurons (5,6). "Hyperphosphorylation" of tau and cleavage of tau by cell proteases (thrombin-like proteases, cathepsins, caspases and calpains) appear to lead to the aggregation of tau into dimers, oligomers, and paired helical filaments (PHFs) which make up the neurofibrillary tangles (NFTs) in patients with Alzheimer's disease (AD) and other tauopathies (7–9). Recent evidence suggests that, while smaller aggregates of tau occur as early events during the course of the disease and are responsible for neurotoxicity, larger filaments and filament bundles are neuroprotective (10–13).

*To whom correspondence should be addressed: Warren J. Goux, Dept. of Chemistry, University of Texas at Dallas, 800 W. Campbell Road, Richardson, TX 75080, Tel: (972) 883-2660; Fax: (972) 883-2925; wgoux@utdallas.edu.

While early work showed recombinant tau and tau isolated from microtubule preparations to be largely unstructured or "natively unfolded", aggregated forms of the protein displayed physical characteristics of amyloid, including a cross-β X-ray diffraction pattern (14–18). Nucleating sequences or "hot spots" in the protein sequence, ^{275}VQIINK (PHF6*) in R2 and ^{306}VQIVYK (PHF6) in R3, were identified, and it has been shown that one or more of these sequences is essential for filament formation (19–22). Previous work from our laboratory has shown that an N- and C-terminal blocked peptide AcPHF6 aggregates into filaments displaying a cross-β-X-ray pattern and, in the presence of smaller peptides, produces twisted filaments with morphology similar to PHFs (23). More recent X-ray work on the PHF6 peptide has shown it to pack in a "steric zipper" with antiparallel layers of parallel, in-register aligned peptides (24–26), while EPR and NMR of tau protein has shown that PHF6 or PHF6 and PHF6* interact intermolecularly in a parallel or antiparallel fashion in protein aggregates (12,27–29). Furthermore, NMR and FRET studies have shown that while the backbone of the protein monomer appears to be in rapid exchange with an ensemble of conformations, the average conformation is one in which the C-terminal is folded over the MTBR and the N-terminal is folded over the C-terminal in a "paperclip" conformation (11,12,30–34). It has been hypothesized that phosphorylation of tau at specific sites opens the paperclip conformation, exposing the MTBR and catalyzing aggregation of the protein or exposing a portion of the N-terminal which inhibits anterograde fast axonal transport, resulting in neurotoxicity (30,35).

Tau lacking the PHF6 still has the ability to form aggregates, implying that PHF6* or other sequences in tau can nucleate tau polymerization or stabilize oligomeric structures (20–22,36). A C-terminal tail peptide that included the PHF6-like sequence ^{392}IVYK^{395} but lacked either PHF6 or PHF6*, was found to form straight filaments containing a high degree of β-sheet conformation (37). While deletion of the C-terminal tail at Lys321 enhances aggregation, a similar deletion at Asp314 renders tau incapable of aggregation, suggesting that ^{314}DLSKVTS is essential for PHF formation. A recent NMR study on full length tau has shown that several other sequences including ^{336}QVEVKSEKLD, ^{86}GKQAAAQ, and ^{224}KKVAVVR are in the β-sheet conformation (31). Surprisingly, deletion of ^{336}QVEVKSE from the MTBR of R4 or the entire R4 sequence enhanced polymerization, suggesting that sequences within R4 have an inhibitory effect (21,38,39).

In a previous study amyloidogenic propensities of individual amino acid residues were extrapolated from measured properties of a family of AcPHF6 peptides (VQIVXK, where X is the substituted residue) using a principal component analysis approach (40). Using individual amino acid propensities, amyloidogenic propensities of sequences within tau conforming to structural motifs, $(X)_nZ$, $Z(X)_nZ$ or $(XZ)_n$ ($n \geq 2$), where X is a hydrophobic residue and Z is a charged or polar amino acid, were estimated. The goal of the present study was to determine if sequences within tau predicted to have high amyloidogenic propensities could, in fact, seed filaments or interact with other known nucleating sequences within the protein (PHF6 and PHF6*). Surprisingly, we found that peptides with these amyloidogenic sequences were able to form all different morphological expressions of amyloid including filaments, tubes, ribbons and rolled sheets. Furthermore, CD difference spectra and kinetics measurements showed that some of these peptides were able to interact with PHF6 or PHF6* peptides in a manner which either enhanced or inhibited aggregation. We found that point mutations in tau which severely reduce the amyloid propensities of these sequences affect the kinetics of aggregation or the number of filaments formed at equilibrium and we interpret these results in terms of inter- and intramolecular interactions.

MATERIALS AND METHODS

Materials

Fmoc-amino acids were purchased from EMD Chemicals (Gibbstown, NJ). High molecular weight heparin (HMWH; porcine mucosa; 18 kDa average MW; 6–30 kDa range) was obtained from Sigma-Aldrich Chemical (St. Louis, MO) and was used without further purification. All other chemicals and buffers were of Reagent grade.

Amyloidogenic propensities of sequences in tau protein

Tau protein was scanned for sequences which satisfied the amphiphilic motifs $(X)_nZ$, $Z(X)_nZ$ or $(XZ)_n$ ($n \geq 2$), where X is a hydrophobic and Z is a polar or charged amino acid residue. Amyloidogenic propensities of sequences satisfying these motifs were evaluated using the sum of the absolute values of their constituent residue PC1 scores (40).

Peptide Synthesis

N-acetyl peptide amides corresponding to potentially nucleating sequences selected in tau were prepared according to previously published procedures and purified by reverse-phase HPLC using a water-acetonitrile gradient (23,40,41). Purity was checked using ESI-MS or MALDI-TOF MS.

Far-UV CD spectroscopy

Stock solutions of the peptides were prepared (~1–5 mg/mL) in deionized water. Final peptide concentrations were determined by absorbance using published molar extinction coefficients for tyrosine [ε_{276} of 1390 $M^{-1}cm^{-1}$] or for the peptide bond [ε_{192} of 7110 $M^{-1}cm^{-1}$](42,43). For CD measurements, peptide stocks were diluted to 100 μM in 5 mM MOPS/0.15 M NaCl, pH 7.2 (MOPS-Cl buffer) containing 0.1 mg/mL of heparin. Samples were transferred to a 0.1 cm path length quartz cell and bath sonicated for 1 min. Far-UV CD spectra were acquired an AVIV 202 CD spectrophotometer, following a 1 h incubation at room temperature in (23,40,44). CD measurements of peptide binary mixtures were prepared in a similar manner with each of the peptides present at 100 μM. In order to calculate mean residue molar ellipticity, the total number of residues was set to the sum of the total number of residues in the peptides included in the mixture.

TEM

Samples for TEM were prepared from peptide stock solutions in MOPS-Cl buffer containing 0.3 mg/mL heparin. Following incubation overnight at room temperature, samples were loaded onto carbon-coated Formvar copper grids (200 mesh) and stained with 2% wt/wt uranyl acetate. A JEOL 1200 EX scope interfaced to a digital camera was used to visualize samples. Distance measurements were made using Adobe Photoshop software (Adobe, Inc., San Jose, CA).

Kinetics of tau peptide aggregation

Polymerization kinetics were measured by monitoring the increase in Thioflavin S (ThS) fluorescence at 490 nm (440 nm excitation) in a manner similar to that used to follow aggregation in other amyloid-forming peptides and proteins (40,41,45–47). For each peptide, a 1 mg/mL sample stock solution was filtered through a Millipore Ultrafree-MC 100,000 NMWL filter unit (Billerica, MA) by centrifuging for 10 minutes at 14,500 rpm, using an Eppendorf MiniSpin plus bench top centrifuge (Westbury, NY). Following filtration, the concentrations of the peptides were determined by UV absorbance. Stock solutions were then diluted in 200 μL wells of a 96-well clear bottom ELISA plate such that the final concentrations were 100 μM peptide, 0.3 mg/mL heparin, 100 μM ThS, in MOPS-

Cl buffer or in 5 mM sodium phosphate containing 0.15 M NaCl, pH 3.0 (phosphate-Cl buffer). Fluorescence data were collected in triplicate in kinetic mode, using a Molecular Devices SPECTRA Max Gemini XPS spectrofluorimeter (Sunnyvale, CA), with measurements taken at 15 s intervals. Mixing between readings was accomplished using a 1/8″ PTFE Grade 2 polished mixing bead (Orange Products, Allentown, PA). In order to minimize time before the first data was collected, peptide solutions were added just before the commencement of the readings. A blank containing only buffer, heparin and ThS was recorded concurrently with the samples. Baseline corrected kinetic data were fit to Gompetz growth curves according to

$$y=e^{-k't}Ae^{-e^{\left(\frac{(t-t_i)}{b}\right)}} \quad [1]$$

where y is defined as the fluorescence signal at time t, t_i corresponds to the inflection point of the curve or the time of maximum growth rate, A is the maximum fluorescence observed for a given sample, and $b = 1/k_{app}$, where k_{app} is the rate constant of aggregation, in units of s^{-1}. The pre-growth curve exponential, $e^{(-k't)}$, was inserted into the traditional Gompetz growth curve equation to take into account the slow decrease in fluorescent intensity resulting from ThS bleaching, quenching and gravitational precipitation of the amyloid-ThS complex (40,48). Each experiment showing peptide aggregation was run 3 times and the error in fitted parameters was determined from the standard deviation of the fitted parameters. Kinetic data for mixtures of some peptides were fit to a sum of growth curve functions according to

$$y=Ae^{-e^{\left(\frac{(t-t')}{b}\right)}}+A'e^{-e^{\left(\frac{(t-t'')}{b'}\right)}} \quad [2]$$

where $b' = 1/k'_{app}$.

2N4R tau experiments

Site directed tau mutants M11K, F378K and Y394K were generated from 2N4R tau (pT7C-htau40 (a gift from Dr. Jeff Kuret)) using the Stratagene QuikChange Site-Directed Mutagenesis kit following manufacturer's protocols. Primers for site-directed mutagenesis were synthesized by Integrated DNA Technologies. The 6x his-tagged proteins were purified using Ni^{2+} charged Chelating Sepharose Fast Flow chromatography, followed by Superdex 200 gel filtration chromatography as previously described (49). 2 μM of wild type or mutants of 2N4R tau (M11K, F378K, and Y394K) were incubated with 75 μM arachidonic acid in polymerization buffer (100 mM NaCl, 10 mM Hepes pH 7.64, 0.1 mM EDTA, 5 mM DTT) for 240 minutes at room temperature. Right angle laser light scattering (LLS) readings were taken at various time points, and images were analyzed by Adobe Photoshop for histogram intensity of the light scattering band (50). Data was fit to the Gompertz growth curve as previously described. A (final extent of polymerization), k_{app} (proportional to the rate of polymerization), and lag (time until significant polymerization), which equals t_i-b, were determined as the mean ± SEM of 3 trials (51). After 240 minutes, reactions were diluted 1:10 and fixed with 10% glutaraldehyde. TEM grids were prepared and filaments were stained with 2% uranyl acetate. Images were collected at 3600x using a Technai F20 XT Field Emission TEM (FEI). Quantitation of 5 TEM images for filament number, length and mass per field was done using Image Pro Plus 6 with a minimum length cutoff of 15 nm.

RESULTS

Amyloidogenic sequences in tau protein

In a previous study we used a family of tau related peptides, AcVQIVXK, to define an amyloidogenic propensity of the amino acid residue X based on a group of experimental observables typically used to define amyloid (40). We found that peptide sequences with an amphiphilic motif $(X)_nZ$, where X is a hydrophobic residue and Z is a charged or polar amino acid, have a high propensity to act as nucleating sequences. Others have shown that amphiphilic sequences in which hydrophobic and polar residues alternate above and below the extended peptide chain ($(XZ)_n$ ($n \geq 2$)) or have a $Z(X)_nZ$ motif also have a high tendency to nucleate amyloid formation (24,52–55). We scanned tau protein for these amyloid-forming motifs and calculated their amyloidogenic propensities using their constituent residue amyloidogenic propensity scores. Using this approach we found 20 high propensity sequences (Fig. 1): 8 sequences (^{5}RQEFEV, ^{10}VME, ^{17}TYGLG, ^{28}GYTMHQDQ, ^{40}DAGLK, ^{87}KQAAAQ, ^{126}RMV, ^{225}K VAVVR) in the N-terminal region, 6 in the microtubule binding region (^{242}RLQ in R1; ^{275}VQIINK (PHF6*) and ^{282}LDLSN in R2; ^{306}VQIVYK (PHF6) in R3; ^{337}VEVK and ^{343}KLDFK in R4), and 6 in the C-terminal region (^{375}KLTFR, ^{382}AKAK, ^{393}VYK, ^{419}MVD, ^{428}LAD, ^{432}VSASL). Of these, PHF6* and PHF6 in the MTBR have been shown experimentally to act as nucleating sequences in tau related peptides or full length tau protein (19).

TEM of predicted amyloid forming sequences in tau

We prepared all 20 predicted amyloidogenic sequences as their N-acetyl peptide amides, since N- and C-terminal charges have been shown to have a profound effect on the ability of a peptide to form amyloid (56). We studied the behavior of these peptides in the presence of HMW heparin, a known polyanion inducer of tau protein aggregation (19,29,45,46,57–60). Using TEM, we observed fibers with diameters between 3 – 7 nm for Ac^{5}RQEFEV, Ac^{40}DAGLK, AcPHF6*, AcPHF6, Ac^{343}KLDFK, Ac^{375}KLTFR, Ac^{393}VYK, and Ac^{419}MVD following overnight incubation in MOPS-Cl buffer with HMW heparin (MOPS-Cl-HMWH; Fig. 2). We also observed tubes, ribbons and rolled sheets for Ac^{10}VME, AcPHF6*, and Ac^{375}KLTFR. TEM data for these peptides can be found in Table 1.

TEM is perhaps the most sensitive measure of the ability of a peptide to form amyloid since the hydrophobic nature of amyloid structures are attracted to the hydrophobic surface of the carbon-coated TEM grid. Previously, we observed amyloid fibers formed from peptides containing proline, a known β-sheet breaking amino acid residue. However, it was later determined by other measurements that the majority of the peptide existed in a random coil conformation (40). Hence, the TEM experiment is biased toward the observation of amyloid-like structures, even when only a relatively small fraction of the sample forms amyloid. Equally important are those sequences that were not observed to form amyloid structures by TEM. These sequences can be eliminated as nucleating sequences and are less likely to affect the kinetics of amyloid formation by their interaction with other nucleating sequences in the protein.

CD of predicted amyloid forming sequences in tau

We used CD spectroscopy to study the conformation of the predicted amyloid forming sequences in tau. In water, the CD of AcPHF6 (Fig. 3A) and AcPHF6* (not shown) displayed a pattern characteristic of random coil peptides with near zero ellipticity at higher wavelength and a single negative band present near 195 nm. Under these conditions these nucleating peptides possess a very low fraction of characteristic of aggregating species having a significant fraction of β-sheet structure. In MOPS-Cl-HMWH, the CD spectra of

AcPHF6* and AcPHF6 showed classical spectra of extended β-sheet, with a negative nπ* band at 217 nm and a positive ππ* band near 198 nm (23,61). With the exception of Ac^{393}VYK and Ac^{10}VME, other peptides studied showed patterns characteristic of random coil peptides in MOPS-Cl-HMWH. The tripeptides Ac^{393}VYK and Ac^{10}VME displayed a CD spectra which appeared to be a combination of spectra arising from β-sheet and random coil structures, having a negative shoulder between 215 and 220 nm and a strong negative band below 198 nm.

We used CD to study the interaction between peptides in MOPS-Cl-HMWH. Figure 3B shows the CD of AcPHF6, Ac^{10}VME, a 1:1 mixture of the two peptides and the CD that would be calculated from the spectra of the peptides by themselves, in the absence of any interaction. As expected, there is a negative 215 nm band for the calculated spectra for AcPHF6 and Ac^{10}VME (dashed line), with an intensity that is half way between that for the spectra of the two peptides alone. In contrast, the observed CD spectrum for a 1:1 mixture of the two peptides (solid line) has a negative 215 nm band with an intensity significantly more negative than the calculated spectrum, suggesting that Ac^{10}VME interacts with AcPHF6 to shift the equilibrium towards the aggregated form. It is also noteworthy that the observed spectrum of the 1:1 mixture shares an isodichroic point at 205 nm with the spectra of the two isolated peptides, suggesting that only two forms of the peptides, monomeric and aggregated, are present (37). A plausible model for this type of interaction is one in which Ac^{10}VME participates in the same β-sheet structure characteristic of the AcPHF6 amyloidogenic state. In contrast, the spectrum of a AcPHF6:AcPHF6* mixture (Fig. 3C) does not appear to share an isodichroic point with spectra of the two pure peptides, suggesting a type of interaction involving something more complex than a simple two state model.

We define a positive interaction as one in which the observed CD of a 1:1 mixture is more negative above (higher wavelength) the isodichroic point and more positive below this point. In contrast, a negative interaction implies that a smaller fraction of the sample exists in an aggregated state when the two peptides are mixed. A summary of the results is presented in Fig. 3D. The greatest positive interactions with AcPHF6 result from peptides Ac^{10}VME, AcPHF6*, Ac^{375}KLTFR and Ac^{393}VYK while the greatest positive interactions with AcPHF6* result from AcPHF6, and from C-terminal sequences Ac^{375}KLTFR, Ac^{393}VYK, Ac^{419}MVD, Ac^{428}LAD, and Ac^{432}VSASL. It should be noted that interactions evaluated in this manner are a reflection of pairwise interactions at thermodynamic equilibrium and do not necessarily reflect how these interactions will affect aggregation kinetics.

Kinetics of tau peptide aggregation

The kinetics of aggregation of tau peptides was measured in MOPS-Cl-HMWH by following the time dependence of ThS fluorescence at 490 nm, and fitting the data to Gompertz growth curves (20,40,41,45,47,48). Under these conditions only AcPHF6 and AcPHF6* displayed measurable aggregation (k_{app} = 23.3±1.4 × 10^{-3} s^{-1} and 9.2±0.7 × 10^{-3} s^{-1}, respectively). We also measured aggregation of these two peptides in the presence of the other predicted amyloidogenic peptides by mixing peptides at a 1:1 stoichiometric ratio. Only Ac^{275}KLTFR had any significant effect on the aggregation ($p \leq 0.05$), slowing the aggregation kinetics of both AcPHF6 and AcPHF6* (19.4 ± 0.5 × 10^{-3} s^{-1} and 3.9 ± 0.6 × 10^{-3} s^{-1}). The effect of Ac^{275}KLTFR on the aggregation of AcPHF6* is shown in Fig. 4A as a function of increasing Ac^{275}KLTFR:AcPHF6* stoichiometry. At less than a 1:1 stoichiometric ratio Ac^{275}KLTFR acts as an aggregation inhibitor, affecting both the k_{app} and the lag time, while at a 2:1 Ac^{275}KLTFR:AcPHF6* stoichiometric ratio there are two discernable aggregation events. Plots of log(k_{app}) and lag time obtained from fitting vs. Ac^{275}KLTFR:AcPHF6* stoichiometry for the first aggregation event showed a linear

relationship (Fig. 5; $r^2 \geq 0.97$), suggesting that both nucleation and elongation are affected in a nucleation-elongation mechanism.

We found it surprising that Ac^{275}KLTFR was an inhibitor of AcPHF6 and AcPHF6* aggregation, but that Ac^{343}KLDFK, a peptide whose sequence is homologous, was not. We hypothesized that it may be the charge-charge repulsion between aspartic acid sidechains that led to its inability to fit into the AcPHF6 or AcPHF6* steric-zipper structure. To test this hypothesis we measured the aggregation of AcPHF6* at different stoichiometric ratios of Ac^{343}KLDFK:AcPHF6* in phosphate buffer at pH 3.0, where the aspartic acid carboxyl is uncharged (Fig. 4B). Under these conditions Ac^{343}KLDFK inhibits the aggregation of AcPHF6* in a dose-dependent manner, similar to the inhibition by Ac^{275}KLTFR at higher pH. A plot of $\log(k_{app})$ vs. Ac^{343}KLDFK:AcPHF6* stoichiometry was linear (Fig. 5A) but we did not observe a linear dependence in lag time with increasing Ac^{343}KLDFK concentration.

Fig. 4C shows the effect that mixing AcPHF6* with AcPHF6 at 1:1 stoichiometry has on aggregation kinetics. Using the same fitted kinetic parameters that we obtained from the kinetics of AcPHF6 and AcPHF6* aggregation, we simulated the aggregation of the AcPHF6:AcPHF6* mixture from a sum of growth curves (dashed line). While the curve comes close to the observed data at short times, it deviates from the data at longer time points. The data could be fit to a sum of growth curves by varying the kinetic parameters for both AcPHF6 and AcPHF6* (solid line) and we found the best fit could be obtained with a significantly faster k_{app} for AcPHF6* ($46 \pm 3 \times 10^{-3}$ s^{-1}) and a significantly slower k_{app} for AcPHF6* ($5.6 \pm 0.6 \times 10^{-3}$ s^{-1}), again suggesting a complex kinetic interaction between these two peptides.

Aggregation kinetics of 2N4R tau mutants

While the CD interaction experiments and kinetic studies on predicted amyloidogenic tau peptides suggest that interactions between sequences may effect tau aggregation rate or the overall fraction of tau participating in an aggregated state, they do not address whether such interactions take place intra- or intermolecularly or what additional constraints the full protein may impose. To address this issue we prepared 3 single site mutants of tau (M11K, F378K, and Y394K) that were predicted to decrease the amyloidogenic propensities of ^{10}VME, ^{275}KLTFR and ^{393}VYK by substituting a positively charged lysine for a hydrophobic residue (40). Kinetics of polymerization for 2N4R lysine mutants were assayed by right angle laser light scattering against wild-type tau (Figure 6A). M11K showed a significantly longer lag time than WT (12.69 ± 3.41 min compared to 7.20 ± 0.61 min; $p \leq 0.05$) while F378K and Y394K showed no significant difference (7.41 ± 0.07 min and 7.22 ± 0.42 min respectively). The k_{app} for M11K decreased significantly (0.09 ± 0.03; $p \leq 0.05$), while the k_{app} for F378K (0.17 ± 0.05) and Y394K (0.15 ± 0.007) were slightly larger than k_{app} for WT (0.13 ± 0.02). M11K, F378K and Y394K showed a trend for slightly higher maximum light scattering values (126.63 ± 18.92, 110.50 ± 13.55, and 113.87 ± 15.16 respectively) than WT (95.40 ± 5.22). TEM images, however, showed no difference in the morphology of filaments (Figure 6B-E). Quantitation of filaments revealed M11K had significantly fewer filaments, while F378K had significantly more filaments ($p \leq 0.0001$) and Y394K had approximately the same number as compared to WT (Figure 6F). Filament lengths were only increased in M11K as compared to WT, with F378K and Y394K having the same average length of filaments per field (Figure 6G). The mass of filaments per field (length × number) was similar to the changes seen for the number of filaments per field (Figure 6H).

DISCUSSION

Whether or not proteins form amyloid depends on the presence of nucleating sequences or "hot spots", short sequences of amino acids that have a high propensity (HP) to form parallel or anti-parallel β-sheet structure between protein monomers (62–65). However, the presence of these nucleating sequences is not a sufficient condition for oligomerization, particularly for most proteins where HP sequences occur on the interior of the protein (63,66). Perturbation of the protein away from its native conformation, either by partial denaturation or by the presence of mutations, controls the exposure of these sequences to the solvent and thus controls their ability to interact intermolecularly with other monomers and form toxic oligomers or filaments (62,64). In "natively unfolded" proteins or peptides, HP sequences may inhibit the formation of amyloid, either by controlling the folding of the backbone or by forming intramolecular β-structure (62,67,68). Tau is a loosely folded flexible protein with two nucleating sequences, PHF6* and PHF6 at the beginning of R2 and R3 in the MTBR (19,31,69). The PHF core is formed by only a portion of tau near the C-terminal, including the MTBR, while N-terminal forms the outer "fuzzy coat" of PHF (14,70–72). Shorter tau related peptides containing PHF6 & PHF6* aggregate much more rapidly than full length tau, suggesting that other segments of the full length protein assume a regulatory role by interacting intramolecularly with the MTBR region (23,40,73). Other segments of tau distant from the nucleating PHF6 and PHF6* regions, such as the N-terminal inserts, tend to promote aggregation (33,38).

Given the evidence suggesting that regions of tau remote from the MTBR are instrumental in regulating polymerization, we were curious to see if (1) HP sequences, other than PHF6 and PHF6*, could nucleate filament formation and (2) HP sequences could interact with the known nucleating sequences PHF6 or PHF6* to increase the fraction of β-sheet structure present or to control aggregation kinetics. We scanned tau for HP motifs and quantitated their propensities using an algorithm previously described by us (40). Other algorithms exist for determining sequence amyloidogenic propensity based on sequence or on their interaction energy with other nucleating sequences (58,74–77). While they are able to find PHF6 and PHF6* in tau, no other potential HP regions have been reported. Our model flagged 20 HP sequences, including ^{87}KQAAAQ, ^{225}KVAVVR, and ^{337}VEVK, in addition to PHF6 and PHF6*. These sequences have previously been shown to populate β-sheet structure by NMR studies of full length tau protein (31). In summary, our simple method of finding potential HP regions of tau is capable of locating sequences that other more complex algorithms can not, although it may be that our method is so sensitive that it flags sequences which neither form amyloid nor interact with other known nucleating sequences.

We used TEM to experimentally evaluate the amyloid forming propensity of N-acetylated peptide amides with sequences identical to the 20 HP sequences in tau flagged by our algorithm. Filaments and tubes were observed for N-terminal peptides Ac^{5}RQEFEV^{10} and Ac^{10}VME. In the past, a Δ2–18 mutant has been shown to aggregate less effectively than wild type tau, suggesting that residues in the N-terminal help seed aggregation in the presence of arachidonic acid inducer (33). Tau with frontotemporal dementia mutation R5L aggregates faster than wild type tau and forms 4.5 times more filaments, again emphasizing the role this segment plays in oligomerization (33). We observed rolled sheets, fibers and ribbons for AcPHF6* and filaments for AcPHF6 and Ac^{343}KLDFK. These sequences occur in the MTBR and have previously been shown by NMR to populate β-sheet structure (31,57,78,79). We observed no amyloid structures for Ac^{87}KQAAAQ, Ac^{225}KVAVVR, or Ac^{337}VEVK, sequences which were observed to populate β-structure in the NMR of full length tau (31). We observed rolled sheets and fiber bundles for Ac^{375}KLTFR, a sequence in tau which lies just downstream of R4, and has been shown by NMR to be in an inflexible region of PHFs (69). We have previously shown that Ac^{393}VYK forms filaments, and

mixtures of AcPHF6 and Ac^{393}VYK form twisted filaments with identical morphology to *bona fide* PHFs (23). The ^{392}IVYK sequence likely is the nucleation sequence for the amyloid formed from the 383-337 C-tail 8 peptide, previously shown to possess a high degree of β-sheet structure and form filaments in the absence of polyanion inducer (37). We also observed fibers and spherical aggregates for the peptide Ac^{419}MVD. Caspase-3 mediated cleavage after Asp421 can be detected in mild cognitive impairment and AD but not in non-demented control brains (7). It is tempting to speculate that C-terminal truncation at this site may allow the ^{419}MVD sequence sufficient solvent accessibility to help seed oligomerization.

Only AcPHF6 and AcPHF6* showed measurable aggregation kinetics as well as a high fraction of β-structure at equilibrium determined by CD. Of the peptides shown by TEM to form amyloid, Ac^{10}VME, AcPHF6*, Ac^{375}KLTFR, and Ac^{393}VYK were found to enhance the fraction of β-structure of AcPHF6 formed at equilibrium, and Ac^{375}KLTFR was found to affect AcPHF6 and AcPHF6* aggregation kinetics. Others have shown that interactions between PHF6 and PHF6* exist in tau or tau related peptides (19–22,27,28). Ac^{375}KLTFR slowed the aggregation kinetics of AcPHF6 by roughly 15% but slowed the k_{app} for AcPHF6* aggregation by 60% at 1:1 stoichiometry. We obtained linear plots of $\log(k_{app})$ or lag time for the first aggregation event versus the Ac^{375}KLTFR/AcPHF6* ratio, suggesting that Ac^{375}KLTFR acts as a competitive inhibitor of AcPHF6* aggregation. Given the sequence homology between Ac^{375}KLTFR and Ac^{343}KLDFK, we found it surprising that Ac^{343}KLDFK was not also an inhibitor of AcPHF6* aggregation. However, we found that Ac^{343}KLDFK was an inhibitor at pH 3.0 where the carboxyl of the aspartic acid sidechain is protonated. Apparently its limited ability to inhibit AcPHF6* aggregation arises from unfavorable interaction between the charged carboxylate sidechains in the peptide at neutral pH. Both Ac^{343}KLDFK and Ac^{375}KLTFR satisfy a model based on the steric-zipper where they occur in alternating layers with AcPHF6*. A hypothetic model shows antiparallel layers of parallel in-register peptide β-structure (Fig. 7) (24,25).

Although data from studies with HP peptides suggest that the sequences ^{10}VME, ^{375}KLTFR and ^{393}VYK have the potential of interacting with PHF6 and PHF6* to enhance the fraction of amyloid present or inhibit the rate of aggregation, it is difficult to predict how these interactions will influence tau aggregation without having some idea of solvent accessibility. Intramolecular interactions which enhance amyloid formation might be expected to inhibit oligomerization while similar intermolecular interactions would be expected to enhance it. In the past, we and others have shown that two consecutive C-terminal positively charged residues transform an amyloidogenic sequence into a non-amyloidogenic one (40,41,55). In the case of the M11K mutant, fewer filaments were observed and there was an increase in lag time and a decrease in the rate of aggregation compared to wild type tau, suggesting that the N-terminal sequence ^{10}VME enhances arachidonic acid induced nucleation and elongation. In contrast, the F378K mutant showed an increased rate of aggregation and more filaments compared to wild type tau. Because of the proximity of the ^{375}KLTFR sequence to PHF6 and PHF6*, it is tempting to speculate that the region just downstream of MTBR interacts intramolecularly with these nucleating sequences, protecting them from interacting intermolecularly. The Y394K mutant produced about the same number of filaments and had a similar rate of aggregation as wild type tau. This result is consistent with NMR evidence which shows that ^{392}IVYK does not form β-structure in full length tau (31,37,59).

In conclusion, we have shown that HP sequences in tau other than PHF6 and PHF6* can nucleate amyloid formation and can help regulate the kinetics of amyloid formation. That being said, amyloid nucleation is a complex event in tau, governed by the folding of the peptide backbone, phosphorylation of amino acid side chains, environmental conditions (reducing or non-reducing, salt concentration, pH), the nature of polyanionic or long chain

fatty acid inducers, and other HP sequences remote from the primary nucleating site (16,31,36,60). These secondary HP sequences in tau or other proteins may have evolved in order to protect biological systems from protein oligomerization and toxicity.

Acknowledgments

2N4R tau (pT7C-htau40) was a gift from Dr. Jeff Kuret.

We would like to thank The University of Texas at Dallas (W.J.G.), The National Institute on Aging grant AG025898 (T.C.G.) and the J.R. and Inez Jay Fund (T.C.G.) for financial support.

Abbreviations

PHF6*	^{275}VQIINK
PHF6	^{306}VQIVYK
PHF	paired helical filament
MTBR	microtubule binding region
R1–R4	32 amino acid pseudorepeats 1 – 4 in the MTBR
DTT	dithioerythritol
MOPS	3-[N-morpholino]propanesulfonic acid
HMWH	hight molecular weight heparin
ThS	thioflavin S
EDTA	ethylene diamine tetracetic acid
SEM	standard error of the mean
HP	high propensity
CD	circular dichroism
TEM	transmission electron microscopy
MALDI-TOF MS	matrix assisted laser desorption/ionization mass spectrometry
ESI	electrospray ionization
FRET	fluorescent resonant energy transfer
PC1 scores	principal component scores
LLS	right angle laser light scattering

References

1. Kosik, KS.; Greenberg, SM. Tau proteins and Alzheimer disease. In: Terry, RD.; Katzman, R.; Bick, KL., editors. Alzheimer Disease. Raven Press; New York: 1994. p. 335-344.
2. Mandelkow EM, Schweers O, Drewes G, Biernat J, Gustke N, Trinczek B, Mandelkow E. Structure, microtubule interactions, and phosphorylation of tau protein. Ann NY Acad Sci. 1996; 777:96–106. [PubMed: 8624133]
3. Friedhoff P, von Bergen M, Mandelkow E-M, Mandelkow E. Structure of tau protein and assembly into paired helical filaments. Biochim Biophys Acta. 2000; 1502:122–132. [PubMed: 10899437]
4. Mandelkow E-M, Mandelkow E. Tau in Alzheimer's disease. Trends Cell Biol. 1998; 8:425–427. [PubMed: 9854307]
5. Jeganathan S, Hascher A, Chinnathambi S, Biernat J, Mandelkow EM, Mandelkow E. Proline-directed pseudo-phosphorylation at AT8 and PHF1 epitopes induces a compaction of the paperclip

folding of tau and generates a pathological (MC-1) conformation. J Biol Chem. 2008; 283:32066–32076. [PubMed: 18725412]

6. Kovacech B, Novak M. Tau truncation is a productive porttranslational modification of neurofibrillary degeneration in Alzheimer's disease. Curr Alz Res. 2010; 7:708–716.
7. Yin H, Kuret J. C-terminal truncation modulates both nucleation and extension phases of τ fibrillization. FEBS Lett. 2006; 580:211–215. [PubMed: 16364303]
8. Khlistunova I, Biernat J, Wang Y, Pickhardt M, von Bergen M, Gazova Z, Mandelkow E, Mandelkow EM. Inducible expression of tau repeat domain in cell models of tauopathy: Aggregation is toxic to cells but can be reversed by inhibitor drugs. J Biol Chem. 2006; 281:1205–1214. [PubMed: 16246844]
9. Wang YP, Biernat J, Pickhardt M, Mandelkow E, Mandelkow EM. Stepwise proteolysis liberates tau fragments that nucleate the Alzheimer-like aggregation of full-length tau in a neuronal cell model. Proc Natl Acad Sci U S A. 2007; 104:10252–10257. [PubMed: 17535890]
10. Meraz-Rios MA, Lira-De León KI, Campos-Peña V, De Anda-Hernández MA, Mena-López R. Tau oligomers and aggregation in Alzheimer's disease. J Neurochem. 2010; 112:1353–1367. [PubMed: 19943854]
11. Mondragón-Rodríguez S, Basurto-Islas G, Binder LI, García-Sierra F. Conformational changes and cleavage; are these responsible for the tau aggregation in Alzheimer's disease? Future Neurol. 2009; 4:39–53.
12. Patterson KR, Remmers C, Fu Y, Srooker S, Kanaan NM, Vana L, Ward W, Reyer JR, Philibert K, Glucksman MJ, Binder LI. Characterization of prefibrillar tau oligomers *in vitro* and in Alzheimer disease. J Biol Chem. 2011; 286:23053–23076.
13. Rankin CA, Gamblin TC. Assessing the toxicity of tau aggregation. J Alz Dis. 2008; 14:411–416.
14. Schweers O, Hanebeck ES, Marx A, Mandelkow E. Structural studies of tau protein and Alzheimer paired helical filaments show no evidence for β-structure. J Biol Chem. 1994; 269:24290–24297. [PubMed: 7929085]
15. von Bergen M, Barghorn S, Biernat J, Mandelkow E-M, Mandelkow E. Tau aggregation is driven by a transition from random coil to β-sheet structure. Biochim Biophys Acta. 2005; 1739:158–166. [PubMed: 15615635]
16. von Bergen M, Barghorn S, Li L, Marx A, Biernat J, Mandelkow EM, Mandelkow E. Mutations of tau protein in frontotemporal dementia promote aggregation of paired helical filaments by enhancing local β-structure. J Biol Chem. 2001; 276:48165–48174. [PubMed: 11606569]
17. Kirschner DA, Abraham C, Selkoe DJ. X-ray diffraction from intraneuronal paired helical filaments and extraneuronal amyloid fibers in Alzheimer disease indicates cross-β conformation. Proc Natl Acad Sci U S A. 1986; 83:503–507. [PubMed: 3455785]
18. Berriman J, Serpell LC, Oberg KA, Fink AL, Goedert M, Crowther RA. Tau filaments from human brain and from *in vitro* assembly of recombinant protein show cross-beta structure. Proc Natl Acad Sci U S A. 2003; 100:9034–9038. [PubMed: 12853572]
19. von Bergen M, Friedhoff P, Biernat J, Heberle J, Mandelkow EM, Mandelkow E. Assembly of τ protein into Alzheimer paired helical filaments depends on a local sequence motif (^{306}VQIVYK^{311}) forming β structure. Proc Natl Acad Sci U S A. 2000; 97:5129–5134. [PubMed: 10805776]
20. Li L, von Bergen M, Mandelkow EM, Mandelkow E. Structure, stability and aggregation of paired helical filaments from tau protein and FTDP-17 mutants probed by tryptophan scanning mutagenesis. J Biol Chem. 2002; 277:41390–41400. [PubMed: 12198126]
21. Li W, Lee M-Y. Characterization of two VQIXXK motifs for tau fibrillization in vitro. Biochemistry. 2006; 45:15692–15701. [PubMed: 17176091]
22. Sahara N, Maeda S, Murayama M, Suzuki T, Dohmae N, Yen SH, Takashima A. Assembly of two distinct dimers and higher-order oligomers from full-length tau. Eur J Neurosci. 2007; 25:3020–3029. [PubMed: 17561815]
23. Goux WJ, Kopplin L, Nguyen AD, Leak K, Rutkofsky M, Shanmuganandam VD, Sharma D, Inouye H, Kirschner DA. The formation of straight and twisted filaments from short tau peptides. J Biol Chem. 2004; 279:26868–26875. [PubMed: 15100221]

24. Sawaya MR, Sambashivan S, Nelson R, Ivanova MI, Sievers SA, Apostol MI, Thompson MJ, Balbirnie M, Wiltzius JJW, McFarlane HT, Madsen AØ, Riekel C, Eisenberg D. Atomic structures of amyloid cross-β spines reveal varied steric zippers. Nature. 2007; 447:453–457. [PubMed: 17468747]
25. Zheng J, Liu C, Sawaya MR, Vadla B, Khan S, Woods JR, Eisenberg D, Goux WJ, Nowick JS. Macrocyclic β-sheet peptides that inhibit the aggregation of a tau-protein-derived hexapeptide. J Am Chem Soc. 2011; 133:3144–3157. [PubMed: 21319744]
26. Sievers SA, Karanicolas J, Chang HW, Zhao A, Jiang L, Zirafi O, Stevens JT, Műch J, Baker D, Eisenberg D. Structure-based design of non-natural amino-acid inhibitors of amyloid fibril formation. Nature. 2011; 475:96–100. [PubMed: 21677644]
27. Margittai M, Langen R. Template-assisted filament growth by parallel stacking of tau. Proc Natl Acad Sci U S A. 2004; 101:10278–10283. [PubMed: 15240881]
28. Peterson DW, Zhou H, Dahlquist FW, Lew J. A soluble oligomer of tau associated with fiber formation analyzed by NMR. Biochemistry. 2008; 47:7393–7404. [PubMed: 18558718]
29. von Bergen M, Barghorn S, Műller SA, Pickhardt M, Biernat J, Mandelkow E-M, Davies P, Aebi U, Mandelkow E. The core of tau-paired helical filaments studied by scanning transmission electron microscopy and limited proteolysis. Biochemistry. 2006; 45:6446–6457. [PubMed: 16700555]
30. Jeganathan S, von Bergen M, Srutlach H, Steinhoff H-J, Mandelkow E. Global hairpin folding of tau in solution. Biochemistry. 2006; 45:2283–2293. [PubMed: 16475817]
31. Mukrasch MD, Bibow S, Korukottu J, Jeganathan S, Biernat J, Griesinger C, Mandelkow E, Zweckstetter M. Structural polymorphism of 441-residue tau at single residue resolution. PLoS Biol. 2009; 7:e34. [PubMed: 19226187]
32. King ME, Gamblin TC, Kuret J, Binder LI. Differential assembly of human tau isoforms in the presence of arachidonic acid. J Neruochem. 2000; 74:1749–1757.
33. Gamblin TC, Berry RW, Binder LI. Tau polymerization: Role of the amino terminus. Biochemistry. 2003; 42:2252–2257. [PubMed: 12590615]
34. Maeda S, Sahara N, Saito Y, Murayama M, Yoshiike Y, Kim H, Miyasaka T, Murayama S, Ikai A, Takashima A. Granular tau oligomers as intermediates of tau filaments. Biochemistry. 2007; 46:3856–3861. [PubMed: 17338548]
35. Kanaan N, Morfini GA, LaPointe NE, Pigino GF, Patterson KR, Song Y, Andreadis A, Fu Y, Brady ST, Binder LI. Pathogenic forms of tau inhibit kinesin-dependent axonal transport through a mechanism involving activation of axonal phosphotransferases. J Neurosci. 2011; 31:9858–9868. [PubMed: 21734277]
36. Lasagna-Reeves CA, Castillo-Carranza DL, Guerrero-Muñoz MJ, Jackson GR, Kayed R. Preparation and characterization of neurotoxic tau oligomers. Biochemistry. 2010; 49:10039–10041. [PubMed: 21047142]
37. Yanagawa H, Chung S-H, Ogawa Y, Sato K, Shibata-Seki T, Masai J, Ishiguro K. Protein Anatomy: C-tail region of human tau protein as a crucial structural element in Alzheimer's paired helical filament formation *in vitro*. Biochemistry. 1998; 37:1979–1988. [PubMed: 9485325]
38. Abraha A, Ghoshal N, Gamblin TC, Cryns V, Berry RW, Kuret J, Binder LI. C-terminal inhibition of tau assembly in vitro and in Alzheimer's disease. J Cell Sci. 2000; 113:3737–3745. [PubMed: 11034902]
39. Sugino E, Nishiura C, Minoura K, In Y, Sumida M, Taniguchi T, Tomoo K, Ishida T. Three-/four-repeat-dependent aggregation profile of tau microtubule-binding domain clarified by dynamic light scattering analysis. Biochem Biophys Res Commun. 2009; 385:236–240. [PubMed: 19450558]
40. Rojas Quijano FA, Morrow D, Wise BM, Brancia FL, Goux WJ. Prediction of nucleating sequences from amyloidogenic propensities of tau-related peptides. Biochemistry. 2006; 45:4638–4652. [PubMed: 16584199]
41. Zhao K, Ippolito G, Wang L, Price V, Kim MH, Cornwell G, Fulenchek S, Breen GA, Goux WJ, D'Mello SR. Neuron-selective toxicity of tau peptide in a cell culture model of neurodegenerative tauopathy: essential role for aggregation in neurotoxicity. J Neurosci Res. 2010; 88:3399–3413. [PubMed: 20882568]

42. Edelhock H. Spectroscopic determination of tryptophan and tyrosine in proteins. Biochemistry. 1967; 6:1948–1954. [PubMed: 6049437]
43. Gill SC, von Hippel PH. Calculation of protein extinction coefficients from amino acid sequence data. Anal Biochem. 1989; 182:319–326. [PubMed: 2610349]
44. Goux WJ. The conformations of filamentous and soluble tau associated with Alzheimer paired helical filaments. Biochemistry. 2002; 41:13798–13806. [PubMed: 12427043]
45. Friedhoff P, Schneider A, Mandelkow EM, Mandelkow E. Rapid assembly of Alzheimer-like paired helical filaments from microtubule-associated protein tau monitored by fluorescence in solution. Biochemistry. 1998; 37:10223–10230. [PubMed: 9665729]
46. Friedhoff P, von Bergen M, Mandelkow EM, Mandelkow E. A nucleated assembly mechanism of Alzheimer paired helical filaments. Proc Natl Acad Sci U S A. 1998; 95:15712–15717. [PubMed: 9861035]
47. LeVine H III. Quantification of beta-sheet amyloid fibril structures with thioflavin T. Methods Enzymol. 1999; 309:274–284. [PubMed: 10507030]
48. Necula M, Kuret J. Pseudophosphorylation and glycation of tau protein enhance but do not trigger fibrillization *in vitro*. J Biol Chem. 2004; 279:49694–49703. [PubMed: 15364924]
49. Rankin CA, Sun Q, Gamblin TC. Pseudo-phosphorylation of tau at Ser202 and Thr205 affects tau filament formation. Brain Res Mol Brain Res. 2005; 138:84–93. [PubMed: 15913837]
50. Voss K, Gamblin TC. GSK-3β phosphorylation of functionally distinct tau isoforms has differential, but mild effects. Mol Neurodegener. 2009; 4:1–12. [PubMed: 19126211]
51. Sun Q, Gamblin TC. Pseudohyperphosphorylation causing AD-like changes in tau has significant effects on its polymerization. Biochemistry. 2009; 48:6002–6011. [PubMed: 19459590]
52. Caplan MR, Moore PN, Zhang S, Kamm RD, Lauffenburger DA. Self-assembly of a β-sheet protein governed by relief of electrostatic repulsion relative to van der Waals attraction. Biomacromolecules. 2000; 1:627–631. [PubMed: 11710192]
53. West MW, Wang W, Patterson J, Mancias JD, Beasley JR, Hect MH. *De novo* amyloid proteins from designed combinatorial libraries. Proc Natl Acad Sci U S A. 1999; 96:11211–11216. [PubMed: 10500156]
54. Zhang S, Rich A. Direct conversion of an oligopeptide from a beta-sheet to an alpha-helix: a model for amyloid formation. Proc Natl Acad Sci U S A. 1997; 94:23–28. [PubMed: 8990154]
55. Blondelle SE, Forood B, Houghten RA, Perez-Paya E. Polyalanine-based peptides as models for self-associated β-pleated-sheet. Biochemistry. 1997; 36:8393–8400. [PubMed: 9204887]
56. Lopez de la Paz M, Goldie K, Zurdo J, Lacroix E, Dobson CM, Hoenger A, Serrano L. De novo designed peptide-based amyloid fibrils. Proc Natl Acad Sci U S A. 2002; 99:16052–16057. [PubMed: 12456886]
57. Carlson SW, Branden M, Voss K, Sun Q, Rankin CA, Gamblin TC. A complex mechanism for inducer mediated tau polymerization. Biochemistry. 2007; 46:8838–8849. [PubMed: 17608454]
58. Mukrasch MD, Biernat J, von Bergen M, Griesinger C, Mandelkow E, Zweckstetter M. Sites of tau important for aggregation populate β-structure and bind to microtubules and polyanions. J Biol Chem. 2005; 280:24978–24986. [PubMed: 15855160]
59. Sibille N, Sillen A, Leroy A, Wieruszeski J-M, Mulloy B, Landrieu I, Lippens G. Structural impact of heparin binding to full-length tau as studied by NMR spectroscopy. Biochemistry. 2006; 45:12560–12572. [PubMed: 17029411]
60. Barghorn S, Mandelkow E. Toward a unified scheme for the aggregation of tau into Alzheimer paired helical filaments. Biochemistry. 2002; 41:14885–1489. [PubMed: 12475237]
61. Woody, RW. Theory of circular dichroism of proteins. In: Fasman, GD., editor. Circular Dichroism and the Conformational Analysis of Biomolecules. Plenum Press; New York: 1996. p. 25-67.
62. Ventura S, Zurdo J, Narayanan S, Parreño M, Mangues R, Reif B, Chiti F, Giannoni E, Dobson CM, Aviles FX, Serrano L. Short amino acid stretches can mediate amyloid formation in globular proteins: the Src homology 3 (SH3) case. Proc Natl Acad Sci U S A. 2004; 101:7258–7263. [PubMed: 15123800]

63. Goldschmidt L, Teng PK, Riek R, Eisenberg D. Identifying the amylome, proteins capable of forming amyloid-like fibrils. Proc Natl Acad Sci U S A. 2010; 107:3487–3492. [PubMed: 20133726]
64. Campioni S, Mannini B, Zampagni M, Pensalfini A, Parrini C, Evangelisti E, Relini A, Stefani M, Dobson CM, Cecchi C, Chiti F. A causative link between the structure of aberrant protein oligomers and their toxicity. Nat Chem Biol. 2010; 6:140–147. [PubMed: 20081829]
65. Teng PK, Eisenberg D. Short protein segments can drive a non-fibrillizing protein into the amyloid state. Prot Eng Des & Sel. 2009; 22:531–536.
66. Chiti F, Taddei N, Baroni F, Capanni C, Stefani M, Ramponi G, Dobson CM. Kinetic partitioning of protein folding and aggregation. Nat Str Biol. 2002; 9:137–143.
67. Brorsson AC, Bolognesi B, Tartaglia GG, Shammas SL, Favrin G, Watson I, Lomas DA, Chiti F, Vendroscolo M, Dobson CM, Crowther DC, Luheshi LM. Intrinsic determinants of neurotoxic aggregate formation by the amyloid β peptide. Biophys J. 2010; 98:1677–1684. [PubMed: 20409489]
68. Scrocchi LA, Ha K, Chen Y, Wu L, Wang F, Fraser PE. Identification of minimal peptide sequences in the (8–20) domain of human islet amyloid polypeptide involved in fibrillogenesis. J Str Biol. 2003; 141:218–227.
69. Sillen A, Leroy A, Wieruszeski J-M, Loyens A, Beauvillain J-C, Bue L, Landrieu I, Lippens G. Regions of tau implicated in the paired helical fragment core as defined by NMR. Chembiochem. 2005; 6:1849–1856. [PubMed: 16196016]
70. Wischik CM, Novak M, Thogersen HC, Edwards PC, Runswick MJ, Jakes R, Walker JE, Milstein C, Roth M, Klug A. Isolation of a fragment of tau derived from the core of paired helical filament of Alzheimer disease. Proc Natl Acad Sci U S A. 1988; 85:4506–4510. [PubMed: 3132715]
71. Ksiezak-Reding H, Wall JS. Characterization of paired helical filaments by scanning transmission electron microscopy. Microsc Res Tech. 2005; 67:126–140. [PubMed: 16104001]
72. Wang YP, Biernat J, Pickhardt M, Mandelkow E, Mandelkow EM. Stepwise proteolysis liberates tau fragments that nucleate the Alzheimer-like aggregation of full-length tau in a neuronal cell model. Proc Natl Acad Sci U S A. 2007; 104:10252–10257. [PubMed: 17535890]
73. Schweers O, Mandelkow EM, Biernat J, Mandelkow E. Oxidation of cysteine-322 in the repeat domain of microtubule-associated protein τ controls the *in vitro* assembly of paired helical filaments. Proc Natl Acad Sci U S A. 1995; 92:8463–8467. [PubMed: 7667312]
74. Pawar AP, Dubay KF, Zurdo J, Chiti F, Vendruscolo M, Dobson CM. Prediction of “aggregation-prone” and “aggregation-susceptible” regions in proteins associated with neurodegenerative diseases. J Mol Biol. 2005; 350:379–392. [PubMed: 15925383]
75. Tartaglia GG, Pawar AP, Campioni S, Dobson CM, Chiti F, Vendroscolo M. Prediction of aggregation-prone regions in structured proteins. J Mol Biol. 2008; 380:425–436. [PubMed: 18514226]
76. Fernandez-Escamilla AM, Rousseau F, Schymkowitz J, Serrano L. Prediction of sequence-dependent and mutational effects on the aggregation of peptides and proteins. Nat Biotechnol. 2004; 22:1302–1306. [PubMed: 15361882]
77. Trovato A, Chiti F, Maritan A, Seno F. Insight into the structure of amyloid fibrils from the analysis of globular proteins. PLoS Comput Biol. 2006; 2:e170. [PubMed: 17173479]
78. Eliezer D, Barré P, Kobaslija M, Chan D, Li X, Heend L. Residual structure in the repeat domain of tau: echoes of microtubule binding and paired helical filament formation. Biochemistry. 2005; 44:1026–1036. [PubMed: 15654759]
79. Andronesi OC, von Bergen M, Biernat J, Seidel K, Griesinger C, Mandelkow E, Baldus M. Characterization of Alzheimer’s-like paired helical filaments from the core domain (K19) of tau protein using solid-state NMR spectroscopy. J Am Chem Soc. 2008; 130:5922–5928. [PubMed: 18386894]

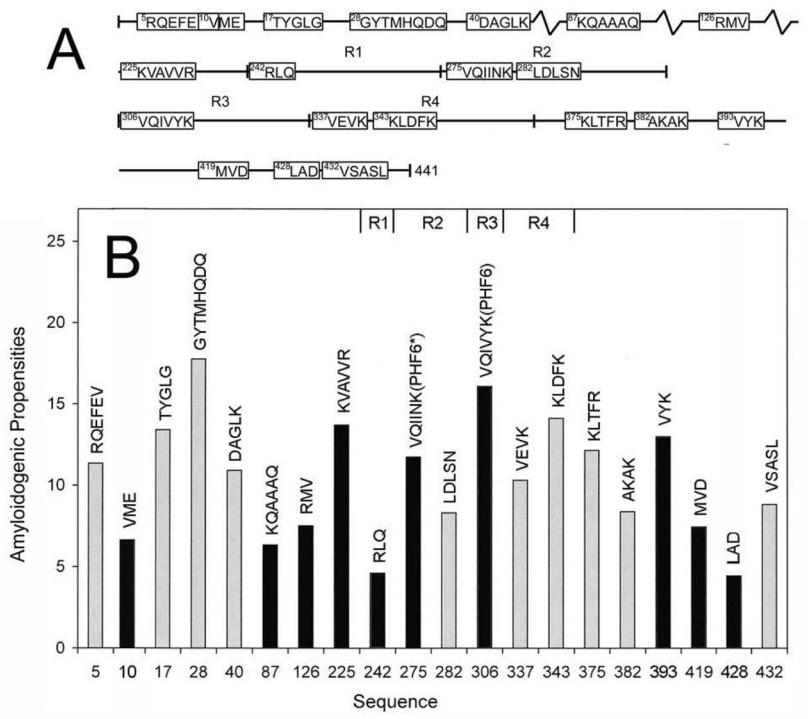

FIG 1.

(A) Schematic of full-length tau showing the 20 sequences which fit the motifs $(X)_nZ$ or $Z(X)_nZ$ (n≥2) or $(XZ)_n$ (n≥2), where X is a hydrophobic residue and Z is a charged or polar amino acid. The model assumes that these sequences have a high propensity to act as nucleating sequences in amyloid formation. (B) Amyloidogenic propensities for sequences calculated by taking the sum of the absolute values of constituent amino acid propensities (40).

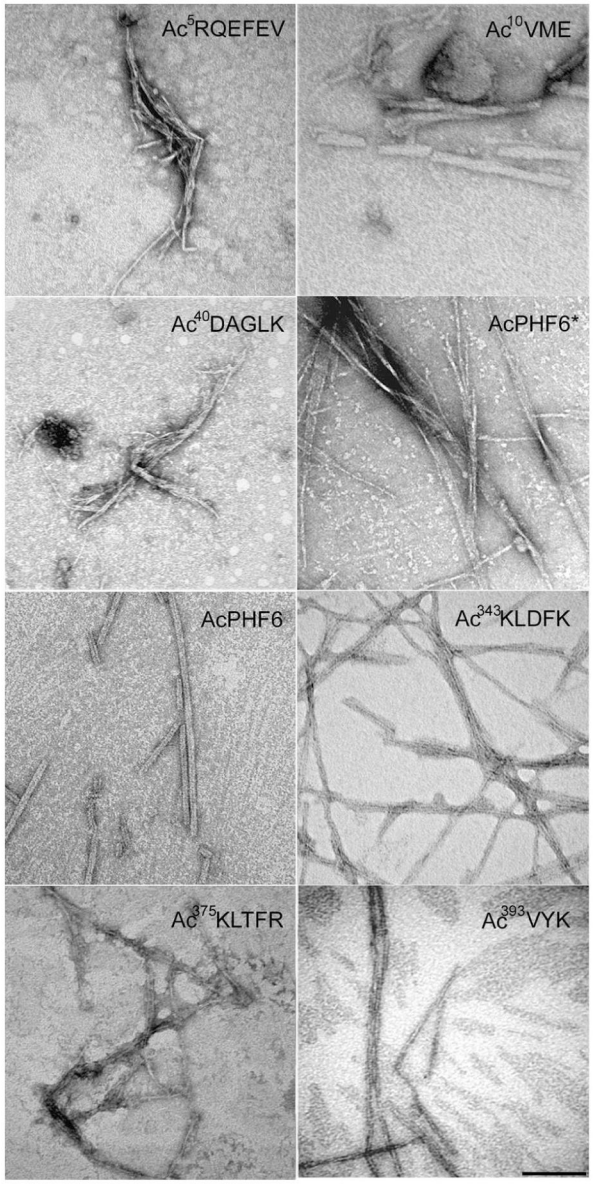

FIG 2.
TEMs of high propensity peptide sequences in MOPS-Cl-HMWH buffer. Scale bar represents 100 nm.

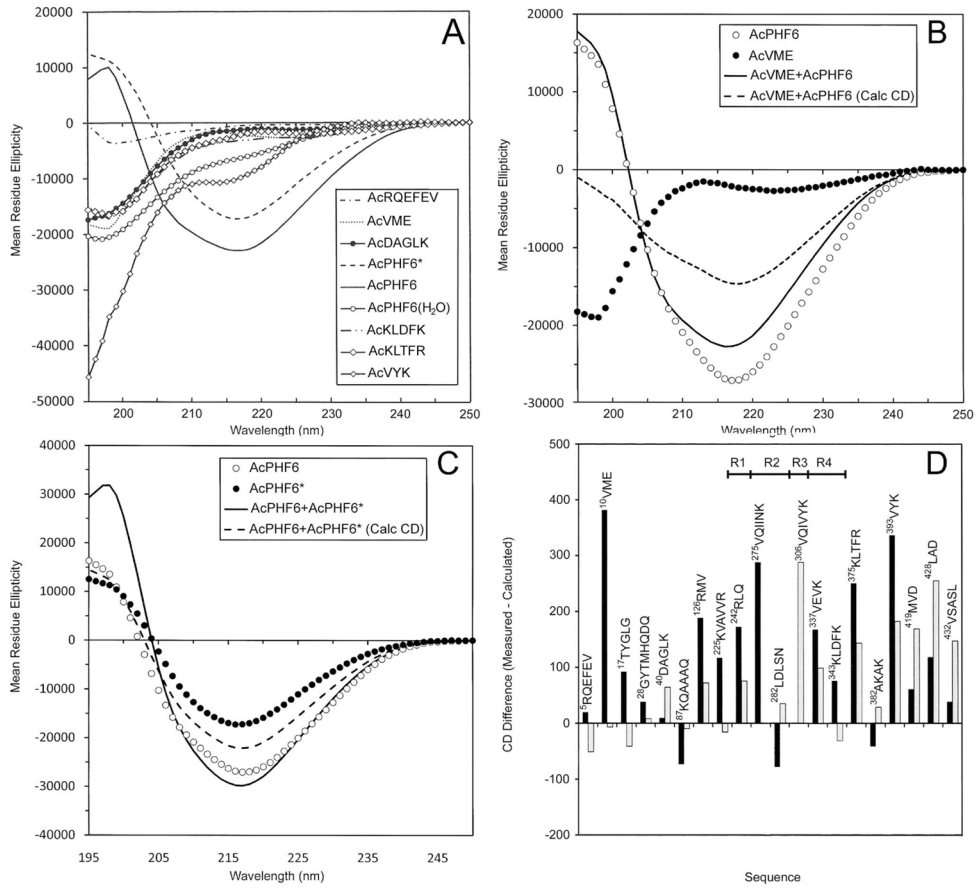

FIG 3.

(A) Far-UV CD spectra of 100 μM N-acetylated peptide amides in water or MOP-Cl-HMWH buffer (pH 7.2). (B) CD of AcPHF6, Ac^{10}VME (MOPS-Cl-HMWH), the calculated mean residue ellipticity of a 1:1 stoichiometric mixture, and the observed ellipticity of the mixture. (C) as in (B) for AcPHF6 and AcPHF6*. (D) Difference between calculated and observed ellipticity for the peptides. A positive interaction is one in which the observed CD of a 1:1 mixture is more negative above (higher wavelength) the isodichroic point and more positive below this point. In contrast, a negative interaction infers that a smaller fraction of the sample exists in an aggregated state when the two peptides are mixed.

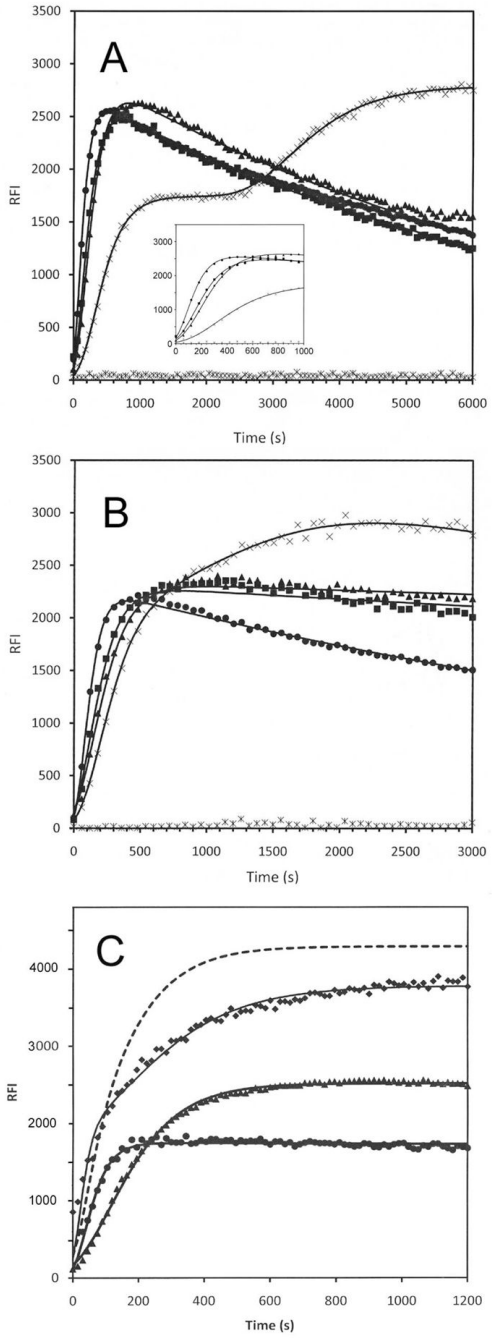

FIG 4.

Aggregation kinetics of peptides and peptide mixtures in MOPS-Cl-HMWH followed by fluorescence of ThS at 490 nm (440 nm excitation). AcPHF6* was 100 μM. (A) AcPHF6* (filled circles), AcPHF6*:Ac^{375}KLTFR at 2:1 (filled squares), 1:1 (filled triangles) and 1:2 stioichiometry (crosses), in MOPS-Cl, pH 7.2. Solid lines represent best fits to the data, assuming a single Gompetz growth curve model for pure AcPHF6* and AcPHF6*:Ac^{375}KLTFR mixtures at less than 1:1 stoichiometry. The AcPHF6*:Ac^{375}KLTFR mixture at 1:2 stoichiometry was modeled using a sum of Gompetz growth curves (Eq. [2]). (B) as in (A) with AcPHF6* and AcPHF6*:Ac^{343}KLDFK mixtures in phosphate-Cl buffer at pH 3.0. (C) Aggregation kinetics of AcPHF6 (filled circles),

AcPHF6* (filled triangles), and a 1:1 stoichiometric mixture of AcPHF6:AcPHF6*. Solid lines represent best fits to a single Gompetz growth curve, in the case of pure peptides, or a sum of two Gompetz growth curves, in the case of the mixture. The dashed line represents a sum of fitted curves for AcPHF6 and AcPHF6*, assuming no interaction between the peptides.

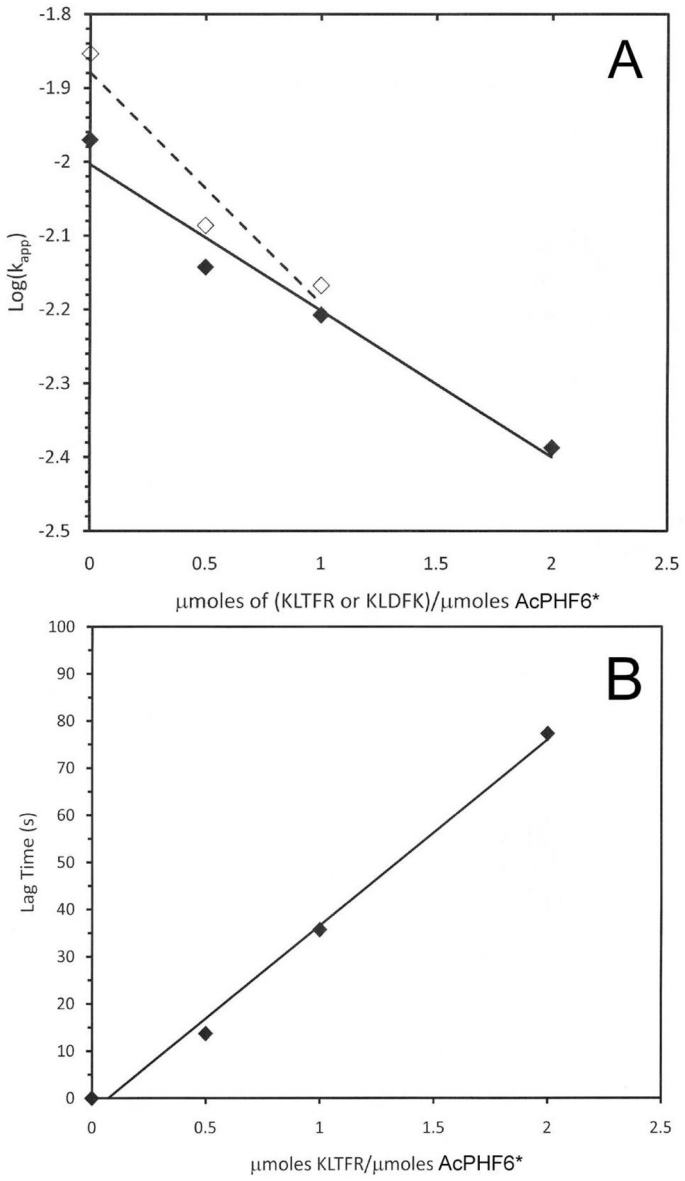

FIG 5.

Plots of parameters obtained from fitting kinetic data for AcPHF6* and AcPHF6*:Ac^{375}KLTFR and AcPHF6*:Ac^{343}KLDFK mixtures. (A) Log(k_{app}) for first aggregation event of AcPHF6* and AcPHF6*:Ac^{375}KLTFR mixtures at pH 7.2 (filled diamonds) and for AcPHF6* and AcPHF6*:Ac^{343}KLDFK mixtures (exempting AcPHF6*:Ac^{343}KLDFK at 1:2 stoichiometry) at pH 3.0 (open diamonds). (B) Lag time for first aggregation event of AcPHF6* and AcPHF6*:Ac^{375}KLTFR mixtures. Data could be fit with an $r^2 > 0.97$.

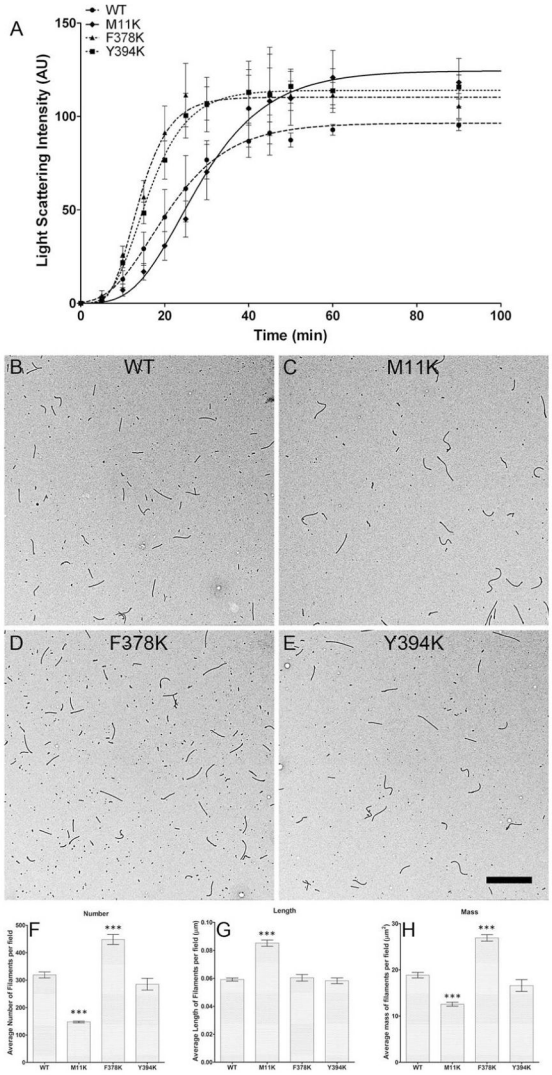

FIG 6.

2N4R lysine mutants show variations from WT tau. Mutant forms (M11K, F378K, and Y394K (diamond, triangle and square respectively)) and WT (circle) 2N4R tau were assayed by LLS over the course of 240 minutes (first 100 minutes shown) (A). Data was fit to the Gompertz growth curve (M11K, F378K, Y394K and WT (solid, long/short dash, short dash and long dashed lines respectively)). Representative TEM images of WT (B), M11K (C), F378K (D), and Y394K (E) were collected at 3600x magnification. Images were quantitated using Image Pro Plus for filament number (F), length (G), and mass (H). Data in F-H are averages of 5 fields ± SEM ($p \leq 0.0001$ for bars marked with asterisks). Scale bar represents 1 μm.

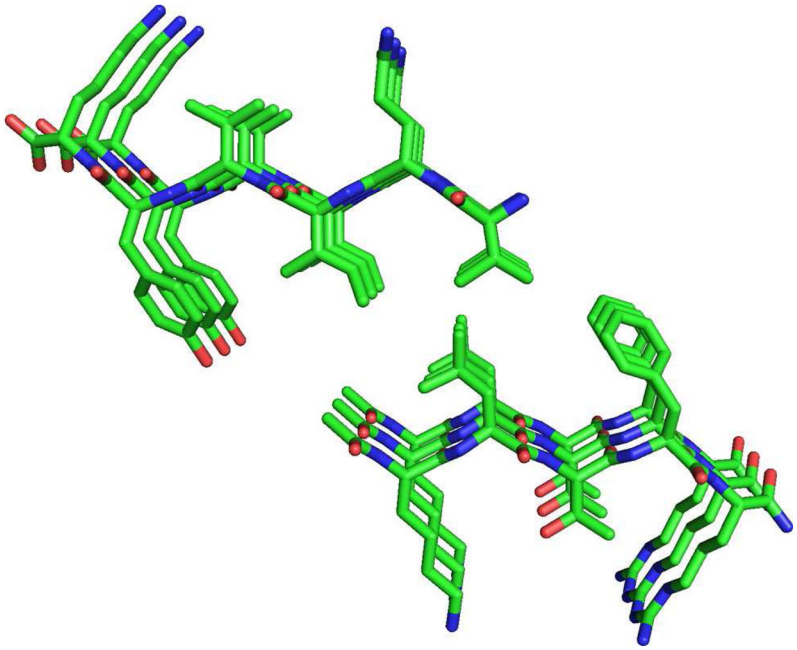

FIG 7.

Hypothetical model for AcPHF6 and Ac^{375}KLTFR in hybrid steric zipper. At 1:1 stoichiometry antiparallel layers of parallel in-register chains of AcPHF6 and Ac^{375}KLTFR continue to form amyloid, albeit at a reduced rate of aggregation.

Table 1

TEM results for tau-related peptides[a]

Peptide	Amyloid Structures	Fiber/Tube Diameter(nm)
Ac^{5}RQEFEV	fiber bundles	2.7 (±0.4)
Ac^{10}VME	tubes	20.3 (±1.5)
Ac^{17}TYGLG	n.o.	
Ac^{28}GYTMHQDQ	n.o.	
Ac^{40}DAGLK	fiber bundles	4.0 (±0.7)
Ac^{126}RMV	n.o.	
Ac^{225}KVAVVR	n.o.	
Ac^{242}RLQ	n.o.	
AcPHF6*	rolled sheets, fibers, ribbons	5.5 (±1.3)
Ac^{282}LDLSN	n.o.	
AcPHF6	fibers	6.5 (±1.2)
Ac^{337}VEVK	n.o.	
Ac^{343}KLDFK	fibers	3.3 (±0.4)
Ac^{375}KLTFR	rolled sheets, fiber bundles	4.0 (±0.9)
Ac^{382}AKAK	n.o.	
Ac^{393}VYK	fibers	5.3 (±0.4)
Ac^{419}MVD	fibers, spherical aggregates	6.8 (±0.4)
Ac^{428}LAD	n.o.	
Ac^{432}VSASL	n.o.	

[a]Results labeled as “n.o.” indicates no amyloid structures were observed.